Published in final edited form as:
J Med Chem. 2010 May 27; 53(10): 4248–4258. doi:10.1021/jm100245q.

Synthesis and Antitumor Activity of 1,5-Disubstituted 1,2,4-Triazoles as Cis-Restricted Combretastatin Analogues

Romeo Romagnoli[*,†], **Pier Giovanni Baraldi**[†], **Olga Cruz-Lopez**[†], **Carlota Lopez Cara**[†], **Maria Dora Carrion**[†], **Andrea Brancale**[‡], **Ernest Hamel**[§], **Longchuan Chen**[‖], **Roberta Bortolozzi**[⊥], **Giuseppe Basso**[⊥], and **Giampietro Viola**[*,⊥]

[†]Dipartimento di Scienze Farmaceutiche, Università di Ferrara, 44100 Ferrara, Italy

[‡]The Welsh School of Pharmacy, Cardiff University, King Edward VII Avenue, Cardiff CF10 3NB, U.K.

[§]Screening Technologies Branch, Developmental Therapeutics Program, Division of Cancer Treatment and Diagnosis, National Cancer Institute at Frederick, National Institutes of Health, Frederick, Maryland 21702

[‖]Department of Pathology, VA Medical Center, Long Beach, California 90822

[⊥]Laboratorio di Oncoematologia, Dipartimento di Pediatria, Università di Padova, 35131 Padova, Italy

Abstract

A series of 1-aryl-5-(3′,4′,5′-trimethoxyphenyl) derivatives and their related 1-(3′,4′,5′-trimethoxyphenyl)-5-aryl-1,2,4-triazoles, designed as cis-restricted combretastatin analogues, were synthesized and evaluated for antiproliferative activity, inhibitory effects on tubulin polymerization, cell cycle effects, and apoptosis induction. Their activity was greater than, or comparable with, that of the reference compound CA-4. Flow cytometry studies showed that HeLa and Jurkat cells treated with the most active compounds **4l** and **4o** were arrested in the G2/M phase of the cell cycle in a concentration dependent manner. This effect was accompanied by apoptosis of the cells, mitochondrial depolarization, generation of reactive oxygen species, activation of caspase-3, and PARP cleavage. Compound **4l** was also shown to have potential antivascular activity, since it induced endothelial cell shape change in vitro and disrupted the sprouting of endothelial cells in the chick aortic ring assay.

Introduction

The microtubule system of eukaryotic cells is a critical element in a variety of fundamental cellular processes, such as cell division, formation and maintenance of cell shape, regulation of motility, cell signaling, secretion, and intracellular transport.[1] Inhibition of microtubule function using tubulin targeting agents, many of which are natural products, is a validated approach for anticancer therapy.[2] One of the most important antimitotic agents is combretastatin A-4 (CA-4,[a] **1**; Chart 1). CA-4, isolated from the bark of the South African tree *Combretum caffrum*,3 is one of the well-known natural tubulin-binding molecules affecting

[*]To whom correspondence should be addressed. For R.R.: phone, 39-(0)532-455303; fax, 39-(0)532-455953. rmr@unife.it. For G.V.: phone, 39-(0)49-8211451; fax, 39-(0)49-8211462. giampietro.viola@unipd.it.

Supporting Information Available: Additional information for synthesis procedures and spectroscopic data for compounds **6a–f,h,i**, **7a–f,h,i**, **3a–f,h–k**, and **4a–f,h–j,m,n,q,r.** This material is available free of charge via the Internet at http://pubs.acs.org.

microtu-bule dynamics by binding to the colchicine site.4 CA-4 shows potent cytotoxicity against a wide variety of human cancer cell lines, including those that are multidrug resistant.[5] A water-soluble disodium phosphate derivative of CA-4 (named CA-4P) has shown promising results in human cancer clinical trials,[6] thus stimulating significant interest in a variety of CA-4 analogues.7

It has been established by previous SAR studies that both the 3′,4′,5′-trimethoxy substitution pattern on the A-ring and the cis-olefin configuration at the bridge were essential for optimal activity, while B-ring structural modifications were tolerated by the target.[7] However, the cis configuration of CA-4 is prone to isomerize to the thermodynamically more stable trans form during storage and administration, producing a dramatic reduction in both antitubulin and antiproliferative activities. Thus, to retain the cis-olefin configuration of CA-4 required for bioactivity, several groups have reported that the isomerization from cis- to trans-olefin can be avoided by incorporating the double bond in five-member aromatic heterocyclic rings, such as pyrazole,[8] imidazole,[9] thiazole,[8] isoxazole,[10] 1,2,3-thiadiazole,[11] isomeric triazoles,[8,12,13] and 1,2,3,4-tetrazole.[8]

Welsh and co-workers reported a series of 3,4-diaryl-1,2,4-triazoles (compounds **2a**–**c**) with antiproliferative activity, but this was 10-fold reduced relative to the activity of CA-4. Nevertheless, these compounds had activity similar to that of CA-4 as inhibitors of tubulin polymerization.[13]

In this article we reconfigured the substitution pattern around the triazole ring by the preparation of two different regioisomeric series of 1,5-diaryl-substituted 1,2,4-triazole derivatives with general structures **3** and **4**. In these two series of designed analogues, obtained by interchanging the substitution pattern of rings A and B, we fixed one of the aryl groups as a 3′,4′,5′-trimethoxyphenyl moiety, identical with the A-ring of CA-4, and examined several substitutions with electron-withdrawing (F, Cl, and NO_2) or electron-releasing (Me, MeO, and EtO) groups (EWG and ERG, respectively) on the other aryl moiety, corresponding to the B-ring of CA-4.

To compare the effect of para-, meta-, and ortho-substitution on compounds with general formula **4**, the methoxy and ethoxy groups were introduced at different positions of the B-phenyl ring to furnish derivatives **4h**–**j** and **4l**–**n**, respectively.

Chemistry

The target 1,5-diaryl-1,2,4-triazoles **3a**–**k** and **4a**–**r** were synthesized as outlined in Scheme 1. 1-Aryl-1,2,4-triazoles **6a**–**i** were prepared by the condensation of the substituted arylhydrazine hydrochlorides **5a**–**i** in formamide at 120 °C. The 1-(3′,4′,5′-trimethoxyphenyl)-1,2,4-triazole **8** was obtained by an efficient N-arylation procedure of 1,2,4-triazole with 1-bromo-3,4,5-trimethoxybenzene catalyzed by CuI and $CsCO_3$.[14] The intermediates **6a**–**i** and **8** were chemoselectively brominated at the 5-position of the 1,2,4-triazole ring by NBS in refluxing CCl_4 to yield derivatives **7a**–**i** and **9**, respectively. The Suzuki cross-coupling reaction with the appropriate arylboronic acid under heterogeneous conditions [$Pd(PPh_3)_4$, K_2CO_3] in refluxing toluene furnished the 1-aryl-5-(3′,4′,5′-trimethoxyphenyl)- and 1-(3′,4′,5′-trimethoxyphenyl)-5-aryl-1,2,4-triazoles **3a**–**i** and **4a**–**r**, respectively. Starting from **3h,i**, the

[a]Abbreviations: CA-4, combretastatin A-4; EWG, electron-withdrawing group; ERG, electron-releasing group; SAR, structure–activity relationship; CuI, copper iodide; $CsCO_3$, cesium carbonate; NBS, *N*-bromo-succinimide; CCl_4, carbon tetrachloride; PI, propidium iodide; PS, phosphatidylserine; HE, hydroethidine; H_2DCFDA, 2,7-dichlorodi-hydrofluorescein diacetate; DCF, dichlorofluorescein; PARP, poly ADP-ribose polymerase; HUVEC, human umbilical vein endothelial cell; GFP, green fluorescent protein; HBSS, Hank's balanced salt solution; PBS, phosphate buffered saline; SDS–PAGE, sodium dodecyl sulfate–polyacrylamide gel electrophoresis.

nitro group was reduced with hydrogen in the presence of 10% Pd/C in DMF, affording amino derivatives **3j,k**, respectively.

The chemoselective bromination at the 5-position of the 1,2,4-triazole ring was unambiguously attributed by ^{1}H–^{1}H NOE experiments on the representative compound **8**. These experiments permit assignment of the signals at 8.489 and 8.085 to the H-5 and H-3 protons, respectively, of the 1,2,4-triazole nucleus. A positive NOE correlation was observed between the signals at 8.489 (H-5) and 6.876 ppm, in which this latter signal corresponds to the aromatic orthoprotons of the 3′,4′,5′-trimethoxyphenyl moiety, and at the same time signals at 8.489 and 6.876 ppm did not show any NOE with the signal at 8.085 ppm.

Results and Discussion

In Vitro Antiproliferative Activities

The series of 1-aryl-5-(3′,4′,5′-trimethoxyphenyl) and their related 1-(3′,4′,5′-trimethoxyphenyl)-5-aryl-1,2,4-triazoles, corresponding to compounds **3a**–**k** and **4a**–**r**, respectively, were evaluated for their antiproliferative activity against a panel of six different human tumor cell lines and compared with the reference compound CA-4 (**1**). Data for inactive compounds (IC_{50} > 10 μM) are not shown in Table 1. Two of the synthesized compounds, **4l** and **4o**, had the best antiproliferative activities against these cell lines and, overall, were as active as CA-4. In particular, the 3′-chloro-4′-ethoxyphenyl derivative **4o** exhibited IC_{50} values ranging from 3 to 20 nM against the cell lines, compared with the range of 4–370 nM obtained with CA-4. It was less active than CA-4 only against the K-562 cells.

Apparently, the relative positions of the two aromatic rings on the 1,2,4-triazole moiety did not seem to be critical for antiproliferative activity. With the exception of the weak activity observed with the *p*-methoxyphenyl derivative **3g**, all the 1-aryl-1,2,4-triazole derivatives **3a**–**k** were inactive (IC_{50} > 10 μM). Switching the position of the two aryls on the 1,2,4-triazole ring (**3a** vs **4a**, **3b** vs **4b**, **3c** vs **4c**, **3d** vs **4d**, **3f** vs **4f**, and **3i** vs **4r**) did not yield active compounds except that there was a considerable difference in potency observed between the regioisomeric 4′-methoxyphenyl derivatives **3g** and **4h** (the latter was considerably more active than the former in four out of the six cell lines).

In the series of 1-(3′,4′,5′-trimethoxyphenyl)-1,2,4-triazole analogues **4h**–**j** and **4l**–**n**, the position of methoxy or ethoxy substituent on the 5-phenyl ring had a profound influence on antiproliferative activity. Starting from compound **4h**, moving the methoxy group from the para- to the meta- and ortho-positions (compounds **4i** and **4j**, respectively) led to a dramatic drop of potency. The same effect was observed for the ethoxy substituent (**4l** vs **4m** and **4n**). The *p*-ethoxy derivative **4l** was 4- to 40-fold more potent than its methoxy counterpart **4h.** The enhanced effect on activity resulting from replacement of the methoxy group with an ethoxy moiety in colchicine site compounds was previously observed by us and by others.[15]

Replacement of the *p*-methoxy group with a weak electron-releasing thiomethyl group resulted in derivative **4k**, which overall had activity similar to that of **4h** against Jurkat and MCF-7 cells. Similarly, except with the K562 cells, replacing the 4′-methoxy of **4h** with a 4′-methyl group (**4g**) overall had only minor effects on antiproliferative activities.

Since the 4′-ethoxy group of **4l** was favorable for potency, it is important to point out that introduction ofan additional EWG chlorine group at the 3′-position of 4′-ethoxyphenyl ring, resulting in compound **4o**, produced a 2- to 15-fold increase in antiproliferative activity against four of the six cell lines, while **4l** and **4o** were equipotent against the Jurkat and K562 cells.

Finally, among the antiproliferative compounds, replacing the 4′-ethoxy group of **4l** with the bulky isopropoxy moiety (**4p**) caused a sharp drop in antiproliferative activity in all cell lines, suggesting that an increase in steric bulk at this position causes a decrease in potency.

Inhibition of Tubulin Polymerization and Colchicine Binding

To investigate whether the antiproliferative activities of compounds **3g**, **4g,h**, **4k,l**, and **4o,p** derived from an interaction with tubulin, they were evaluated for their inhibition of tubulin polymerization and for effects on the binding of [^{3}H]colchicine to tubulin (Table 2).[16] For comparison, CA-4 was examined in contemporaneous experiments. In the assembly assay, compound **4l** was found to be the most active (IC_{50} = 0.76 μM), and it was almost twice as potent as CA-4 (IC_{50} = 1.2 μM). While **4l** was generally less potent than **4o** as an antiproliferative agent, **4l** was about twice as active as **4o** as an inhibitor of tubulin assembly. Derivative **4o** was also slightly less active than CA-4 as an inhibitor of tubulin assembly. Compound **4h** was the next most active agent as an inhibitor of tubulin assembly (about half as potent as CA-4). The remaining compounds with lower antiproliferative effects on cancer cells were still less active as inhibitors of tubulin assembly. For these seven compounds and CA-4, the order of activity was **4l** > CA-4 > **4o** > **4h** > **4k** > **4g** > **4p** ≫ **3g**.

In the colchicine binding studies, derivative **4l** was as potent as CA-4, which in these experiments inhibited colchicine binding by 87%, while **4o** was slightly less potent (75% inhibition). The potent inhibition observed with the two compounds indicates that **4l** and **4o** bind to tubulin at a site overlapping the colchicine site. Inhibition of colchicine binding by compounds **4g,h**, **4k**, and **4p** fell into the 33–55% range. In this series of seven compounds, inhibition of [^{3}H]colchicine binding correlated more closely with inhibition of tubulin assembly than with antiproliferative activity. In conclusion, we note that CA-4 is one of the most potent colchicine compounds yet described. It is thus significant that two agents in the present series have activities comparable to that CA-4 as inhibitors of tubulin assembly and, less frequently observed, as inhibitors of colchicine binding to tubulin.

Analysis of Cell Cycle

The effects of different concentrations of compounds **4l** and **4o** on cell cycle progression were examined with HeLa and Jurkat cells (Figure 1). Untreated HeLa cells showed a classical pattern of proliferating cells distributed in the G1 (55.2%), S (32.4%), and G2/M (12.4%) phases. Both **4l** and **4o** caused a clear G2/M arrest pattern in a concentration-dependent manner, with a concomitant decrease of cells in other phases of the cell cycle (Figure 1). In particular, as shown in Figure 2 (upper panels), the G2/M cell population increased from 12% in the control to over 70% with 30 nM compounds **4l** and **4o** at 48 h.

In the leukemia T-cell Jurkat line, both compounds also induced a significant block in the G2/M phase. With both cell lines, the accumulation of G2/M cells increased to varying extents in a time-dependent manner (Figure 2). In addition, treatment of cells with **4l** or **4o** caused the appearance of a hypodiploid peak (sub-G1) indicative of apoptosis (data not shown).

Loss of Plasma Membrane Asymmetry during Apoptosis

To better characterize drug-induced apoptosis, we performed a biparametric cytofluorimetric analysis using propidium iodide (PI) and annexin-V-FITC, which stain DNA and phosphatidylserine (PS) residues, respectively.[17] Annexin-V is a Ca^{2+}-dependent phospholipid binding protein with high affinity for PS. Annexin-V staining precedes the loss of membrane integrity that accompanies the final stages of cell death resulting from either apoptotic or necrotic processes. Because the externalization of PS occurs in the earlier stages of apoptosis, annexin-V staining identifies apoptosis at an earlier stage than the appearance of sub-G1 cells.

These cells appear at a later stage of cell death and indicate the occurrence of nuclear changes such as DNA fragmentation.

After treatment with **4l** and **4o** at 50 nM for different times, Jurkat cells were labeled with the two dyes, and the resulting red (PI) and green (FITC) fluorescence was monitored by flow cytometry. It can be observed from Figure 3 that **4l** and **4o** provoked a significant induction of apoptotic cells after 24 h of treatment. The percentage of annexin-V positive cells then further increased at 48 and 72 h. These findings prompted us to further investigate the apoptotic process after treatment with the two compounds.

Induction of Mitochondrial Depolarization

Mitochondria play an essential role in the propagation of apoptosis.[18] It is well established that at an early stage apoptotic stimuli alter the mitochondrial transmembrane potential ($\Delta\psi_{mt}$). $\Delta\psi_{mt}$ was monitored by the fluorescence of the dye JC-1.[19] With normal cells (high $\Delta\psi_{mt}$), JC-1 displays a red fluorescence (590 nm). This is caused by spontaneous and local formation of aggregates that is associated with a large shift in the emission. In contrast, when the mitochondrial membrane is depolarized (low $\Delta\psi_{mt}$), JC-1 forms monomers that emit at 530 nm. Treated Jurkat cells in the presence of derivatives **4l** and **4o** (50 nM) exhibited a remarkable shift in fluorescence compared with control cells, indicating depolarization of the mitochondrial membrane potential (Figure 4, upper panels). The percentage of cells with low $\Delta\psi_{mt}$ following treatment increased in a time-dependent fashion (Figure 4, lower panel). The disruption of $\Delta\psi_{mt}$ is associated with the appearance of annexin-V positivity in the treated cells when they are in an early apoptotic stage. In fact, the dissipation of $\Delta\psi_{mt}$ is characteristic of apoptosis and has been observed with both microtubule stabilizing and destabilizing agents, including CA-4, in different cell types.[20]

Mitochondrial Generation of Reactive Oxygen Species (ROS)

Mitochondrial membrane depolarization is associated with mitochondrial production of ROS.[21] Therefore, we investigated whether ROS production increased after treatment with the test compounds. We utilized the fluorescence indicator hydroethidine (HE), whose fluorescence appears if ROS are generated.[22] HE is oxidized by superoxide anion into the ethidium ion, which fluoresces red. Superoxide is produced by mitochondria because of a shift from the normal four-electron reduction of O_2 to a one-electron reduction when cytochrome *c* is released from mitochondria. ROS generation was also measured with the dye 2,7-dichlorodihydrofluorescein diacetate (H_2-DCFDA), which is oxidized to the fluorescent compound dichlorofluorescein (DCF) by a variety of peroxides, including hydrogen peroxide.[22]

The results are presented in Figure 5, where it can be observed that **4l** and **4o** induced the production of large amounts of ROS in comparison with control cells, which agrees with the previously described dissipation of $\Delta\psi_{mt}$. The amount of ROS produced increased over the entire 72 h treatment time.

Caspase-3 Activation, Poly ADP-Ribose Polymerase (PARP) Cleavage, and Bcl-2 Down-Regulation

Caspases are the central executioners of apoptosis mediated by various inducers.[23] Caspases are synthesized as proenzymes that are activated by cleavage. Caspases-2, -8, -9, and -10 are termed apical caspases and are usually the first to be stimulated in the apoptotic process. Their activation in turn leads to their activation of effector caspases, in particular caspase-3.[24] Exposure of Jurkat cells to compound **4l** or **4o** resulted in the activation of caspase-3 in a time-dependent manner, as shown in Figure 6.

PARP is a 116 kDa nuclear protein that appears to be involved in apoptosis.[25] This protein is one of the main cleavage targets of caspase-3 both in vitro and in vivo.[25] As shown in Figure 7 (top panel), immunoblot analysis demonstrated extensive formation of the typical 89 kDa fragment of PARP following a 24 h treatment with either 50 nM **4l** or 50 nM **4o.** There was a further increase, especially with **4o**, after treatment for another 24 h, most noticeable through disappearance of uncleaved PARP. Similar results were obtained with CA-4 in HeLa cells.[20b]

Bcl-2 is a protein that has been extensively investigated as a modulating agent of apoptosis and plays a major role as an inhibitor of apoptosis. It does this by regulating the mitochondrial membrane potential, thus avoiding release of cytochrome c and caspase activation.[26] Therefore, we examined whether the induction of apoptosis by **4o** and **4l** is associated with changes in the expression of this protein. As depicted in Figure 7 (middle panel), immunoblot analysis showed that treatment with either compound resulted in decreased expression of Bcl-2. Altogether these data indicate that the induction of apoptosis by these new derivatives is associated with Bcl-2 down-regulation and caspase-3 activation that in turn stimulated PARP cleavage.

Antivascular Activity

CA-4 and its analogues in clinical development have been shown to quickly and selectively shut down the blood flow of tumors.6a,b This family of drugs is therefore called antivascular or vascular disrupting agents. The effect is thought to be mediated by inducing endothelial cell shape change, possibly through disrupting microtubule dynamics.[27] We tested the derivative **4l** for its ability to induce rapid endothelial cell shape changes using a human umbilical vein endothelial cell (HUVEC) culture assay and a chick aortic ring assay.[28] The HUVEC line expressed green fluorescent protein (GFP). In these model systems, we found that changes occurred rapidly and were extensive 30 min after drug addition, corresponding to the quick in vivo effect of shutting down tumor circulation. Like CA-4, **4l** caused spreading HUVECs to retract and form blebs on their membranes at a concentration as low as 0.5 μM, and the effect was prominent at 10 μM. The area of GFP positive HUVECs was reduced to 30% of the area measured before treatment (Figure 8). Compound **4l** also disrupted formation of vascular sprouts from chick aortic ring after only a 30 min incubation. These observations suggest that **4l**, like CA-4, would most likely cause severe vascular disruption in vitro and it could be considered as a new vascular disrupting agent.

Molecular Modeling Studies

To rationalize the experimental data obtained, molecular docking studies were performed on this series of compounds. The docking pose observed for **4l** showed a very similar binding mode to the cocrystallized DAMA-colchicine[29] with the trimethoxyphe-nyl ring in close contact to Cys 241 (residue numbering derived from the crystal structure used) and the other aromatic moiety placed deep in the binding pocket (Figure 9). These results are in accordance with the observed experimental results; in particular, the ethoxy group is placed in a tight hydrophobic region, which does not seem able to accommodate a bulkier group, explaining the loss in activity of compound **4p**. It should also be noted that the methoxy analogue **4h** does not occupy this hydrophobic area as efficiently as **4l**, possibly explaining the reduced biological activity observed for **4h.** Furthermore, in the case of **4o**, the chlorine atom in position 3 of the aromatic ring is placed in the same position as the carbonyl group of DAMA-colchi-cine, and also in this case, only relatively small groups should be tolerated in this position. In further support of this model is the inactivity of compounds **4i** and **4m**, which have a methoxy group and an ethoxy group, respectively, at position 3 of the aromatic ring. These compounds could not be docked successfully in the colchicine binding site.

Conclusions

In conclusion, we proposed that the 1,5-diarylsubstituted 1,2,4-triazole ring could serve as a suitable mimic to retain the bioactive configuration afforded by the cis-double bond present in CA-4. In the present study, we fixed one of the aryl groups as a 3′,4′,5′-trimethoxyphenyl moiety, and the modifications were mainly focused on variation of the substituents on the second phenyl ring. It is clear that the substitution pattern on the phenyl at the 5-position of the 1,2,4-triazole ring plays an important role for antitubulin and antiprolifera-tive activities, and this was supported by the molecular docking studies. The results demonstrated that either the 4′-ethoxy (**4l**) substituent or the 4′-ethoxy and 3′-chloro (**4o**) substitu-ents on the second phenyl ring could replace the B-ring of CA-4, at least with a 1,2,4-triazole ring as the bridge. Both these derivatives exhibited potent tubulin polymerization inhibitory activity as well as antiproliferative activity, comparable with that of CA-4. Compound **4l** was the most potent inhibitor of tubulin polymerization and one of the most potent inhibitors of colchicine binding (IC_{50} = 0.76 μM for assembly, 86% inhibition of the binding of [^{3}H]colchicine). We also showed by flow cytometry that **4l** and **4o** had cellular effects typical for microtubule-interacting agents, causing accumulation of cells in the G2/M phase of the cell cycle. Further studies showed that **4l** and **4o** are potent inducers of apoptosis in the Jurkat cell line. Apoptosis induced by antimitotic agents has been associated with alteration in a variety of cellular signaling pathway. As with many antimitotic drugs, compounds **4l** and **4o** are able to induce Bcl-2 down-regulation just after 24 h of treatment. Bcl-2 prevents the initiation of the cellular apoptotic program by stabilizing mitochondrial permeability. The loss of $\Delta\psi_{mt}$ results in an uncoupling of the respiratory chain and the efflux of small molecules such as caspase-9 and the apoptosis-inducing factor (AIF), which in turn can stimulate proteolytic activation of caspase-3. Our results confirm that the induction of apoptosis by **4l** and **4o** is associated with down-regulation of Bcl-2, dissipation of the mitochondrial transmembrane potential, and activation of caspase-3, which is coupled with terminal events of apoptosis such as PARP cleavage. Finally, preliminary experiments have assessed the potential antivascular activity of compound **4l.** The ability of this compound to inhibit vascular sprouting is consistent with antivascular agent utility and warrants further testing in preclinical in vivo cancer models.

Experimental Section

Chemistry

Materials and Methods—^{1}H NMR spectra were recorded on a Bruker AC 200 spectrometer. Chemical shifts (δ) are given in ppm upfield from tetramethylsilane as internal standard, and the spectra were recorded in appropriate deuterated solvents, as indicated. Positive-ion electrospray ionization (ESI) mass spectra were recorded on a double-focusing Finnigan MAT 95 instrument with BE geometry. Melting points (mp) were determined on a Buchi-Tottoli apparatus and are uncorrected. All products reported showed ^{1}H NMR spectra in agreement with the assigned structures. The purity of tested compounds was determined by combustion elemental analyses conducted by the Microanalytical Laboratory of the Department of Chemistry of the University of Ferrara with a Yanagimoto MT-5 CHN recorder elemental analyzer. All tested compounds yielded data consistent with a purity of at least 95% compared with the theoretical values. All reactions were carried out under an inert atmosphere of dry nitrogen, unless otherwise indicated. Standard syringe techniques were used for transferring dry solvents. Reaction courses and product mixtures were routinely monitored by TLC on silica gel (precoated F_{254} Merck plates), and compounds were visualized with aqueous $KMnO_4$. Flash chromatography was performed using 230–400 mesh silica gel and the indicated solvent system. Organic solutions were dried over anhydrous Na_2SO_4. Arylhydrazine hydrochlorides **5a**–**i** and arylboronic acids are commercially available and used as received.

General Procedure A for the Synthesis of 1-Aryl-1*H*-[1,2,4]-triazoles 6a–i—A suspension of the appropriate arylhydrazine hydrochloride (10 mmol) in 10 mL of formamide was heated at 120 °C for 12 h. The mixture was cooled and dissolved in a mixture of ethyl acetate (20 mL) and water (10 mL). The organic layer was washed with water (3 × 10 mL), brine (10 mL), dried (Na_2SO_4), filtered, and concentrated to give a residue purified by column chromatography on silica gel.

1-(4-Methoxyphenyl)-1*H*-1,2,4-triazole (6g)—Following general procedure A, compound **6g** was purified by chromatogra-phy, eluting with petroleum ether–EtOAc (1:1). Brown solid, yield 71%, mp 88–89 °C. ^{1}H NMR ($CDCl_3$) δ: 3.88 (s, 3H), 7.03 (d, *J* = 9.0 Hz, 2H), 7.58 (d, *J* = 9.0 Hz, 2H), 8.10 (s, 1H), 8.47 (s, 1H).

Synthesis of 1-(3,4,5-Trimethoxyphenyl)-1 *H*-1,2,4-triazole (8)—To a round-bottom flask charged with CuI (382 mg, 2 mmol) were added $CsCO_3$ (6.52 g., 20 mmol), 1,2,4-triazole (1 g, 14.5 mmol), 3,4,5-trimethoxyphenylboronic acid (2.47 g, 10 mmol), and DMF (20 mL) under nitrogen. The system was then evacuated twice, backfilled with nitrogen, and heated at 120 °C for 24 h. The reaction mixture was then cooled to room temperature and diluted with EtOAc (20 mL) and water (10 mL). The aqueous phase was filtered on a pad of Celite, and the filtrate was washed with EtOAc (2 × 10 mL). The combined organic extracts were washed with brine (10 mL), dried over Na_2SO_4, and concentrated. The resulting residue was purified by column chromatog-raphy on silica gel (EtOAc) to provide **8** as a white solid. Yield 78%, mp 119–121 °C. ^{1}H NMR ($CDCl_3$) δ: 3.88 (s, 3H), 3.93 (s, 6H), 6.88 (s, 2H), 8.09 (s, 1H), 8.49 (s, 1H). Anal. ($C_{17}H_{17}N_3O_3$) C, H, N.

General Procedure B for the Synthesis of 1-Aryl-5-bromo-1*H*-[1,2,4]triazoles (7a–i) and 1-(3,4,5-Trimethoxyphenyl)-5-bromo-1*H*-[1,2,4]triazoles (9)—To a suspension of the appropriate 1-aryl-1*H*-[1,2,4]triazole **6a**–**i** or 1-(3,4,5-trimethoxyphenyl)-1*H*-1,2,4-triazole **9** (3 mmol) in 15 mL of CCl_4 were added NBS (1.07 g, 6 mmol) and a catalytic amount of benzoyl peroxide (72 mg, 0.3 mmol). The solution was heated to reflux for 12 h, then cooled and filtered through Celite, washing the solids with warm CCl_4 (5 mL). The solvent was removed in vacuo and the residue purified by column chromatography on silica gel.

5-Bromo-1-(4-methoxyphenyl)-1*H*-1,2,4-triazole (7g)—Following general procedure B, compound **7g** was purified by chromatography, eluting with petroleum ether–EtOAc (8:2). Gray solid, yield 52%, mp 103–105 °C. ^{1}H NMR ($CDCl_3$) δ: 3.88 (s, 3H), 7.02 (d, *J* = 6.8 Hz, 2H), 7.44 (d, *J* = 6.8 Hz, 2H), 8.01 (s, 1H).

5-Bromo-1-(3,4,5-trimethoxyphenyl)-1*H*-1,2,4-triazole (9)—Following general procedure B, compound **9** was purified by chromatography, eluting with petroleum ether–EtOAc (3:7). Yellow solid, yield 68%, mp 182–184 °C. ^{1}H NMR ($CDCl_3$) δ: 3.89 (s, 3H), 3.90 (s, 6H), 6.75 (s, 2H), 8.02 (s, 1H).

General Procedure C (Suzuki Coupling) for the Synthesis of Compounds 3a–i and 4a–r—A mixture of 5-bromo-1-aryl-1*H*-[1,2,4]triazoles **7a**–**i** or 1-(3,4,5-trimethoxyphenyl)-5-bro-mo-1*H*-1,2,4-triazole **9** (0.5 mmol), potassium carbonate (104 mg, 0.75 mmol, 1.5 equiv), the appropriate arylboronic acid (1 mmol, 2 equiv), and tetrakis (triphenylphosphine)palladium (13.5 mg, 0.012 mmol) in dry toluene (10 mL) was stirred at 100 °C under nitrogen for 18 h, cooled to ambient temperature, filtered through Celite, and evaporated in vacuo. The residue was dissolved with EtOAc (30 mL), and the resultant solution was washed sequentially with 5% $NaHCO_3$ (10 mL), water (10 mL), and brine (10 mL). The

organic layer was dried, filtered, and evaporated, and the residue was purified by flash chromatography on silica gel.

1-(4-Methoxyphenyl)-5-(3,4,5-trimethoxyphenyl)-1-(4-methoxyphenyl)-1*H*-1,2,4-triazole (3g)—Following general procedure C, compound **3g** was purified by chromatography, eluting with petroleum ether–EtOAc (6:4). Yellow solid, yield 58%, mp 117–119 °C. ^{1}H NMR ($CDCl_3$) δ: 3.67 (s, 6H), 3.85 (s, 3H), 3.86 (s, 3H), 6.74 (s, 2H), 6.96 (d, *J* = 9.0 Hz, 2H), 7.31 (d, *J* = 9.0 Hz, 2H), 8.05 (s, 1H). MS (ESI): $[M]^+$ = 341.8. Anal. ($C_{18}H_{19}N_3O_4$) C, H, N.

1-(3,4,5-Trimethoxyphenyl)-5-*p*-tolyl-1*H*-1,2,4-triazole (4g)—Following general procedure C, compound **4g** was purified by chromatography, eluting with petroleum ether–EtOAc (1:1). White solid, yield 55%, mp 106–108 °C. ^{1}H NMR ($CDCl_3$) δ: 2.36 (s, 3H), 3.73 (s, 6H), 3.88 (s, 3H), 6.56 (s, 2H), 7.22 (d, *J* = 8.4 Hz, 2H), 7.42 (d, *J* =8.4 Hz, 2H), 8.06 (s, 1H). **MS (ESI): $[M + 1]^+$ = 326.5. Anal. ($C_{18}H_{19}N_3O_3$)C, H, N.

1-(3,4,5-Trimethoxyphenyl)-5-(4-methoxyphenyl)-1*H*-1,2,4-triazole (4h)—Following general procedure C, compound **4h** was purified by chromatography, eluting with petroleum ether–EtOAc (1:1). White solid, yield 56%, mp 72–74 °C. ^{1}H NMR ($CDCl_3$) δ: 3.75 (s, 6H), 3.86 (s, 3H), 3.88 (s, 3H), 6.58 (s, 2H), 6.90 (d, *J* = 9.0 Hz, 2H), 7.48 (d, *J* = 9.0 Hz, 2H), 8.04 (s, 1H). MS (ESI): $[M]^+$ = 341.7. Anal. ($C_{18}H_{19}N_3O_4$) C, H, N.

1-(3,4,5-Trimethoxyphenyl)-5-(4-(methylthio)phenyl)-1*H*-1,2,4-triazole (4k)—Following general procedure C, compound **4k** was purified by chromatography, eluting with petroleum ether–EtOAc (1:1). White solid, yield 86%, mp 123–125 °C. ^{1}H NMR ($CDCl_3$) δ: 2.48 (s, 3H), 3.74 (s, 6H), 3.88 (s, 3H), 6.56 (s, 2H), 7.18 (d, *J* = 8.6 Hz, 2H), 7.44 (d, *J* = 8.6 Hz, 2H), 8.02 (s, 1H). MS (ESI): $[M]^+$=357.3. Anal. ($C_{18}H_{19}N_3O_3S$) C, H, N.

1-(3,4,5-Trimethoxyphenyl)-5-(4-ethoxyphenyl)-1*H*-1,2,4-triazole (4l)—Following general procedure C, compound **4l** was purified by chromatography, eluting with petroleum ether–EtOAc (1:1). White solid, yield 55%, mp 107–109 °C. ^{1}H NMR ($CDCl_3$) δ:1.42(t, *J* = 7.0 Hz, 3H), 3.75 (s, 6H), 3.88 (s, 3H), 4.02 (q, *J* = 7.0 Hz, 2H), 6.58 (s, 2H), 6.84 (d, *J* = 8.8 Hz, 2H), 7.46 (d, *J* = 8.8 Hz, 2H), 8.04 (s, 1H). MS (ESI): $[M + H]^+$ = 356.0. Anal. ($C_{19}H_{21}N_3O_4$) C, H, N.

5-(3-Chloro-4-ethoxyphenyl)-1-(3,4,5-trimethoxyphenyl)-1*H*-1,2,4-triazole (4o)—Following general procedure C, compound **4o** was purified by chromatography, eluting with petroleum ether–EtOAc (1:1). Yellow solid, yield 56%, mp 107–109 °C. ^{1}H NMR ($CDCl_3$) δ: 1.47 (t, *J* = 7.2 Hz, 3H), 3.76 (s, 6H), 3.88 (s, 3H), 4.12 (q, *J* = 7.2 Hz, 2H), 6.56 (s, 2H), 6.84 (d, *J* =8.6 Hz, 1H), 7.30 (d, *J* = 8.6 Hz, 1H), 7.69 (s, 1H), 8.04 (s, 1H). MS (ESI): $[M + H]^+$ = 390.6. Anal. ($C_{19}H_{20}ClN_3O_4$)C, H, N.

5-(4-Isopropoxyphenyl)-1-(3,4,5-trimethoxyphenyl)-1*H*-1,2,4-triazole (4p)—Following general procedure C, compound **4p** was purified by chromatography, eluting with petroleum ether–EtOAc (1:1). White solid, yield 83%, mp 120–122 °C. ^{1}H NMR ($CDCl_3$) δ: 1.31 (d, *J* = 6.2 Hz, 6H), 3.74 (s, 6H), 3.88 (s, 3H), 4.57 (m, 1H), 6.58 (s, 2H), 6.85 (d, *J* = 9.2 Hz, 2H), 7.45 (d, *J* = 9.2 Hz, 2H), 8.03 (s, 1H). MS (ESI): $[M + 1]^+$ = 370.2. Anal. ($C_{20}H_{23}N_3O_4$)C, H, N.

General Procedure D for the Synthesis of 3j–k—A solution of the appropriate nitrophenyl derivative **7h,i** (0.25 mmol) in DMF (5 mL) was hydrogenated over 35 mg of 10%

Pd/C at 60 psi for 2 h. The catalyst was removed by filtration on Celite, and the filtrate was concentrated to give a residue which was purified by column chromatography on silica gel.

Biology

Materials and Methods

Antiproliferative Assays: Human T-leukemia (Jurkat), human promyelocytic leukemia (HL-60), and human chronic myelogenous leukemia (K562) cells were grown in RPMI-1640 medium (Gibco Milano, Italy). Breast adenocarcinoma (MCF7), human nonsmall lung carcinoma (A549) and human cervix carcinoma (HeLa) cells were grown in DMEM medium (Gibco, Milano, Italy), all supplemented with 115 units/mL of penicillin G (Gibco, Milano, Italy), 115 μg/mL streptomycin (Invitrogen, Milano, Italy) and 10% fetal bovine serum (Invitrogen, Milano, Italy). Individual wells of a 96-well tissue culture microtiter plate were inoculated with 100 μL of complete medium containing 8×10^3 cells. The plates were incubated at 37 °C in a humidified 5% CO_2 incubator for 18 h prior to the experiments. After medium removal, 100 μL of the drug solution, dissolved in complete medium at different concentrations, was added to each well and incubated at 37 °C for 72 h. Cell viability was assayed by the (3-(4,5-dimethylthiazol-2-yl)-2,5-diphenyltetrazolium bromide (MTT) test as previously described.[30] The IC_{50} was defined as the compound concentration required to inhibit cell proliferation by 50%.

Effects on Tubulin Polymerization and on Colchicine Binding to Tubulin: To evaluate the effect of the compounds on tubulin assembly in vitro,[16a] varying concentrations of compounds were preincubated with 10 μM bovine brain tubulin in glutamate buffer at 30 °C and then cooled to 0 °C. After addition of 0.4 mM GTP, the mixtures were transferred to 0 °C cuvettes in a recording spectrophotometer and warmed to 30 °C. Tubulin assembly was followed turbidimetrically at 350 nm. The $IC_{50}$was defined as the compound concentration that inhibited the extent of assembly by 50% after a 20 min incubation. The capacity of the test compounds to inhibit colchicine binding to tubulin was measured as described[16b] except that the reaction mixtures contained 1 μM tubulin, 5 μM [^{3}H]colchicine, and 1 μM test compound.

Flow Cytometric Analysis of Cell Cycle Distribution and Apoptosis: For flow cytometric analysis of DNA content, 5×10^5 HeLa or Jurkat cells in exponential growth were treated with different concentrations of the test compounds for 24 and 48 h. After an incubation period, the cells were collected, centrifuged, and fixed with ice-cold ethanol (70%). The cells were then treated with lysis buffer containing RNase A and 0.1% Triton X-100 and stained with PI. Samples were analyzed on a Cytomic FC500 flow cytometer (Beckman Coulter). DNA histograms were analyzed using MultiCycle for Windows (Phoenix Flow Systems).

Annexin-V Assay: Surface exposure of PS on apoptotic cells was measured by flow cytometry with a Coulter Cytomics FC500 (Beckman Coulter) by adding annexin-V-FITC to cells according to the manufacturer's instructions (Annexin-V Fluos, Roche Diagnostic). Simultaneously the cells were stained with PI. Excitation was set at 488 nm, and the emission filters were at 525 and 585 nm, respectively.

Assessment of Mitochondrial Changes: The mitochondrial membrane potential was measured with the lipophilic cation 5,5′,6,6′-tetrachloro-1,1′,3,3′-tetraethylbenzimidazolcarbocyanine (JC-1, Molecular Probes), as described.19،30 Briefly, after different times of treatment, the cells were collected by centri-fugation and resuspended in Hank's balanced salt solution (HBSS) containing 1 μM JC-1. The cells were then incubated for 10 min at 37 °C, centrifuged, and resuspended in HBSS. The production of ROS was measured by flow cytometry using either HE (Molecular Probes) or H_2DCFDA (Molecular Probes).

After different times of treatment, cells were collected by centrifugation and resuspended in HBSS containing the fluorescence probe HE or H_2DCFDA at 2.5 or 0.1 μM, respectively. The cells were then incubated for 30 min at 37 °C, centrifuged, and resuspended in HBSS. The fluorescence was directly recorded with the flow cytometer, using an excitation wavelength of 488 nm and emission wavelengths of 585 and 530 nm for HE and H_2DCFDA, respectively.

Caspase-3 Assay: Caspase-3 activation in Jurkat cells was evaluated by flow cytometry using a human active caspase-3 fragment antibody conjugated with FITC (BD Pharmingen). Briefly, after different incubation times in the presence of test compounds, the cells were collected by centrifugation and resuspended in Cytofix (BD Pharmingen) buffer for 20 min, washed with Perm/Wash (BD Pharmingen), and then incubated for 30 min with the antibody. After this period, cells were washed and analyzed by flow cytometry. Results are expressed as percentage of caspase-3 active fragment positive cells.

Western Blot Analysis: Jurkat cells were incubated in the presence of test compounds and, after different times, were collected, centrifuged, and washed two times with ice cold phosphate buffered saline (PBS). The pellet was then resuspended in lysis buffer. After the cells were lysed on ice for 30 min, lysates were centrifuged at 15000*g* at 4 °C for 10 min. The protein concentration in the supernatant was determined using the BCA protein assay reagents (Pierce, Italy). Equal amounts of protein (20 μg) were resolved using sodium dodecyl sulfate–polyacrylamide gel electrophoresis (SDS–PAGE) (7.5–15% acrylamide gels) and transferred to a PVDF Hybond-p membrane (GE Healthcare). Membranes were blocked with I-block (Tropix), and the membrane was gently rotated overnight at 4 °C. Membranes were then incubated with primary antibodies against Bcl-2, PARP (all rabbit, 1:1000, Cell Signaling), or β-actin (mouse, 1:10,000, Sigma) for 2 h at room temperature. Membranes were next incubated with peroxidase-labeled goat antirabbit IgG (1:100000, Sigma) or peroxidase-labeled goat antimouse IgG (1:100000, Sigma) for 60 min. All membranes were visualized using ECL Advance (GE Healthcare) and exposed to Hyperfilm MP (GE Healthcare). To ensure equal protein loading, each membrane was stripped and reprobed with an anti-β-actin antibody.

Endothelial Cell Shape Change Assays: HUVECs expressing GFP (green fluorescence protein) were cultured in EGM-2 media with endothelial cell growth supplement and transferred into 18-well μ-Slide plates coated with collagen 1 day before assay. Cell morphology and GFP fluorescence were recorded in a Nikon confocal microscope with an imaging system before and after drug additions at different time points. The area of HUVECs with GFP was further analyzed by the imaging software MetaMorph (Molecular Devices). The chick aortic ring assay was performed as described in ref 28. Briefly, aortic arches were dissected from day 14 chick embryos, cut into cross-sectional slices, and implanted in 10 μL of Matrigel (Becton Dickinson) in eight-well Lac-Tek chamber slides with complete media. Endothelial cell sprouts or channels were formed in 24–48 h. Various concentrations of 4 L were added, and images of the vascular channels were captured with a digital camera before and 30 min after drug addition.

Molecular Modeling: All molecular modeling studies were performed on a MacPro dual 2.66 GHz Xeon computer running Ubuntu 8. The tubulin structure was downloaded from the PDB data bank (http://www.rcsb.org/; PDB code 1SA0).[30] Hydrogen atoms were added to the protein, using Molecular Operating Environment (MOE),[31] and minimized keeping all the heavy atoms fixed until a rmsd gradient of 0.05 kcal mol^{-1} $Å^{-1}$ was reached. Ligand structures were built with MOE and minimized using the MMFF94x force field until a rmsd gradient of 0.05 kcal mol^{-1} $Å^{-1}$ was reached. The docking simulations were performed using PLANTS.[32]

Supplementary Material

Refer to Web version on PubMed Central for supplementary material.

References

1. a Amos LA. Microtubule structure and its stabilisation. Org. Biomol. Chem 2004;2:2153–2160. [PubMed: 15280946] b Walczak CE. Microtubule dynamics and tubulin interacting proteins. Curr. Opin. Cell. Biol 2000;12:52–56. [PubMed: 10679354]
2. a Mahindroo N, Liou JP, Chang JY, Hsieh HP. Antitubulin agents for the treatment of cancer. A medicinal chemistry update. Expert Opin. Ther. Pat 2006;16:647–691. b Jordan MA, Wilson L. Microtubules as a target for anticancer drugs. Nat. Rev. Cancer 2004;4:253–265. [PubMed: 15057285] c Hadfield JA, Ducki S, Hirst N, McGown AT. Tubulin and microtubules as targets for anticancer drugs. Prog. Cell Cycle Res 2003;5:309–325. [PubMed: 14593726] d Honore S, Pasquier E, Braguer D. Understanding microtubule dynamics for improved cancer therapy. Cell. Mol. Life. Sci 2005;62:3039–3065. [PubMed: 16314924] e Pellegrini F, Budman DR. Review: tubulin function, action of antitubulin drugs, and new drug development. Cancer Invest 2005;23:264–273. [PubMed: 15948296] f Attard G, Greystoke A, Kaye S, De Bono J. Update on tubulin binding agents. Pathol. Biol 2006;54:72–84. [PubMed: 16545633] g Lawrence NJ, McGown AT. The chemistry and biology of antimitotic chalcones and related enone systems. Curr. Pharm. Des 2005;11:1679–1693. [PubMed: 15892668]
3. Pettit GR, Singh SB, Hamel E, Lin CM, Alberts DS, Garcia-Kendall D. Isolation and structure of the strong cell growth and tubulin inhibitor combretastatin A-4. Experentia 1989;45:209–211.
4. Lin CM, Ho HH, Pettit GR, Hamel E. Antimitotic natural products combretastatin A-4 and combretastatin A-2: studies on the mechanism of their inhibition of the binding of colchicine to tubulin. Biochemistry 1989;28:6984–6991. [PubMed: 2819042]
5. McGown AT, Fox BW. Differential cytotoxicity of combretastatins A1 and A4 in two daunorubucin-resistant P388 cell lines. Cancer Chemother. Pharmacol 1990;26:79–81. [PubMed: 2322992]
6. a Grosios K, Holwell SE, McGown AT, Pettit GR, Bibby MC. In vivo and in vitro evaluation of combretastatin A-4 and its sodium phosphate prodrug. Br. J. Cancer 1999;81:1318–1327. [PubMed: 10604728] b Vincent L, Kermani P, Young LM, Cheng J, Zhang F, Shido K, Lam G, Bompais-Vincent H, Zhu Z, Hicklin DJ, Bohlen P, Chaplin DJ, May C, Rafii S. Combretastatin A4 phosphate induces rapid regression of tumor neovessels and growth through interference with vascular endothelial-cadherin signaling. J. Clin. Invest 2005;115:2992–3006. [PubMed: 16224539] c Chaplin DJ, Hill SA. The development of combretastatin A4 phosphate as a vascular targetingagent. Int. J. Radiat. Oncol., Biol., Phys 2002;54:1491–1496. [PubMed: 12459376] d Young SL, Chaplin DJ. Combretastatin A-4 phosphate: background and current clinical status. Expert Opin. Invest. Drugs 2004;13:1171–1182. e Bilenker JH, Flaherty KT, Rosen M, Davis L, Gallagher M, Stevenson JP, Sun W, Vaughn D, Giantonio B, Zimmer R, Scnall M, O'Dwyer PJ. Phase I trial of combretastatin A-4 phospate with carboplatin. Clin. Cancer Res 2005;11:1527–1533. [PubMed: 15746056]
7. a Nam NH. Combretastatin A-4 analogues as antimitotic antitumor agents. Curr. Med. Chem 2003;10:1697–1722. [PubMed: 12871118] b Chaudari A, Pandeya SN, Kumar P, Sharma PP, Gupta S, Soni N, Verma KK, Bhardwaj G. Combretastain A-4 analogues as anticancer agents. Mini-Rev. Med. Chem 2007;12:1186–1205. c Tron GC, Pirali T, Sorba G, Pagliai F, Busacca S, Genazzani AA. Medicinal chemistry of combretastatin A4: present and future directions. J. Med. Chem 2006;49:3033–3044. [PubMed: 16722619] d Gaukroger K, Hadfield JA, Lawrence NJ, Nlan S, McGown AT. Structural requirements for the interaction of combretastatins with tubulin: how important is the trimethoxy unit? Org. Biomol. Chem 2003;1:3033–3037. [PubMed: 14518125] e Hatanaka T, Fujita K, Ohsumi K, Nakagawa R, Fukuda Y, Nihei Y, Suga Y, Akiyama Y, Tsuji T. Novel B-ring modified combretastatin analogues: synthesis and antineoplastic activity. Bioorg. Med. Chem. Lett 1998;8:3371–3374. [PubMed: 9873736]
8. Ohsumi K, Hatanaka T, Fujita K, Nakagawa R, Fukuda Y, Nihai Y, Suga Y, Morinaga Y, Akiyama Y, Tsuji T. Synthesis and antitumor activity of cis-restricted combretastatins 5-membered heterocyclic analogues. Bioorg. Med. Chem. Lett 1988;8:3153–3158. [PubMed: 9873694]
9. a Bellina F, Cauteruccio S, Monti S, Rossi R. Novel imidazole-based combretastatin A-4 analogues. Evaluation of their in vitro antitumor activity and molecular modeling study of their binding to the

colchicine site of tubulin. Bioorg. Med. Chem. Lett 2000;16:5757–5762. [PubMed: 16950621] b Wang L, Woods KW, Li Q, Barr KJ, McCroskey RW, Hannick SM, Gherke L, Credo RB, Hui Y-H, Marsh K, Warner R, Lee JY, Zielinski-Mozng N, Frost D, Rosenberg SH, Sham HL. Potent, orally active heterocycle-based combretastatin A-4 analogues: synthesis, structure–activity relationship, pharmacokinetics, and in vivo antitumor activity evaluation. J. Med. Chem 2002;45:1697–1711. [PubMed: 11931625]

10. Kaffy J, Pontikis R, Carrez D, Croisy A, Monneret C, Florent J-C. Isoxazole-type derivatives related to combretastatin A-4, synthesis and biological evaluation. Bioorg. Med. Chem 2006;14:4067–4077. [PubMed: 16510288]
11. Wu M, Li W, Yang C, Chen D, Ding J, Chen Y, Lin L, Xie Y. Synthesis and activity of combretastatin A-4 analogues: 1,2,3-thiadiazoles as potent antitumor agents. Bioorg. Med. Chem. Lett 2007;17:869–873. [PubMed: 17174089]
12. Odlo K, Hentzen J, Fournier dit Chabert J, Ducki S, Gani OABSM, Sylte I, Skrede M, Florenes VA, Hansen TV. 1,5-Disubstituted 1,2,3-triazoles as cis-restricted analogues of combretastatin A-4: synthesis, molecular modeling and evaluation as cytotoxic agents and inhibitors of tubulin. Bioorg. Med. Chem 2008;16:4829–4838. [PubMed: 18396050]
13. Zhang Q, Peng Y, Wang XI, Keeman SM, Aurora S, Welsh WJ. Highly potent triazole-based tubulin polymerization inhibitors. J. Med. Chem 2007;50:749–754. [PubMed: 17249649]
14. Zhu L, Guo P, Li G, Lan J, Xie R, You J. Simple copper salt-catalyzed N-arylation of nitrogen-containing heterocycles with aryl and heteroaryl halides. J. Org. Chem 2007;72:8535–8538. [PubMed: 17902694]
15. a Romagnoli R, Pier Baraldi PG, Carrion MD, Cruz-Lopez O, Lopez Cara C, Tolomeo M, Grimaudo S, Di Cristina A, Pipitone MR, Balzarini J, Zonta N, Brancale A, Hamel E. Design, synthesis and structure–activity relationship of 2-(3′,4′,5′-trimethoxybenzoyl)-benzo[*b*]furan derivatives as a novel class of antitubulin agents. Bioorg. Med. Chem 2009;17:6862–6871. [PubMed: 19736015] b Cushman M, He H-M, Katzenellenbogen JA, Hamel E. Synthesis, antitubulin and antimitotic activity and cytotoxicity of analogs of 2-meth-oxyestradiol, an endogenous mammalian metabolite of estradiol that inhibits tubulin polymerization by binding to the colchicine. J. Med. Chem 1995;38:2041. [PubMed: 7783135] c Kim S, Min SY, Lee SK, Cho W-J. Comparative molecular field analysis study of stilbene derivatives active against A549 lung carcinoma. Chem. Pharm. Bull 2003;51:516–521. [PubMed: 12736450]
16. a Hamel E. Evaluation of antimitotic agents by quantitative comparisons of their effects on the polymerization of purified tubulin. Cell Biochem. Biophys 2003;38:1–21. [PubMed: 12663938] b Verdier-Pinard P, Lai J-Y, Yoo H-D, Yu J, Marquez B, Nagle DG, Nambu M, White JD, Falck JR, Gerwick WH, Day BW, Hamel E. Structure–activity analysis of the interaction of curacin A, the potent colchicine site antimitotic agent, with tubulin and effects of analogs on the growth of MCF-7 breast cancer cells. Mol. Pharmacol 1998;53:62–67. [PubMed: 9443933]
17. Vermes I, Haanen C, Steffens-Nakken H, Reutelingsperger C. A novel assay for apoptosis. Flow cytometric detection of phos-phatidylserine expression on early apoptotic cells using fluorescein labelled annexin V. J. Immunol. Methods 1995;184:39–51. [PubMed: 7622868]
18. a Ly JD, Grubb DR, Lawen A. The mitochondrial membrane potential ($\Delta\psi_m$) in apoptosis: an update. Apoptosis 2003;3:115–128. [PubMed: 12766472] b Green DR, Kroemer G. The pathophysiology of mitochondrial cell death. Science 2005;305:626–629. [PubMed: 15286356]
19. Salvioli S, Ardizzoni A, Franceschi C, Cossarizza A. JC-1 but not DiOC6(3) or rhodamine 123 is a reliable fluorescent probe to assess ΔΨ changes in intact cells: implications for studies on mitochondrial functionality during apoptosis. FEBS Lett 1997;411:77–82. [PubMed: 9247146]
20. a Mollinedo F, Gajate C. Microtubules, microtubule-interfering agents and apoptosis. Apoptosis 2003;8:413–450. [PubMed: 12975575] b Vitale I, Antoccia A, Cenciarelli C, Crateri P, Meschini S, Arancia G, Pisano C, Tanzarella C. Combretastatin CA-4 and combretastatin derivative induce mitotic catastrophe dependent on spindle checkpoint and caspase-3 activation in non-small cell lung cancer cells. Apoptosis 2007;12:155–166. [PubMed: 17143747]
21. Zamzami N, Marchetti P, Castedo M, Decaudin D, Macho A, Hirsch T, Susin SA, Petit PX, Mignotte B, Kroemer G. Sequential reduction of mitochondrial transmembrane potential and generation of reactive oxygen species in early programmed cell death. J. Exp. Med 1995;182:367–377. [PubMed: 7629499]

22. a Rothe G, Valet G. Flow cytometric analysis of respiratory burst activity in phagocytes with hydroethidine and 2′,7′-dichloro-fluorescein. J. Leukocyte Biol 1990;47:440–448. [PubMed: 2159514] b Cai J, Jones DP. Superoxide in apoptosis. Mitochondrial generation triggered by cytochrome c loss. J. Biol. Chem 1998;273:11401–11404. [PubMed: 9565547] c Nohl H, Gille L, Staniek K. Intracellular generation of reactive oxygen species by mitochondria. Biochem. Pharmacol 2005;69:719–723. [PubMed: 15710349]
23. a Thomberry AN, Lazebnik Y. Caspases: enemies within. Science 1998;281:1312–1316. [PubMed: 9721091] b Earshaw WC, Martins LM, Kaufmann SH. Mammalian caspases: structure, activation, substrates and functions during apoptosis. Annu. Rev. Biochem 1999;68:383–424. [PubMed: 10872455] c Reed JC. Apoptosis-based therapies. Nat. Rev. Drug Discovery 2002;1:111–121. d Denault J-B, Salvesen GS. Caspases: keys in the ignition of cell death. Chem. Rev 2002;102:4489–4499. [PubMed: 12475198]
24. Porter AG, Janicke RU. Emerging role of caspase-3 in apoptosis. Cell Death Differ 1999;6:99–104. [PubMed: 10200555]
25. Soldani C, Scovassi AI. Poly(ADP-ribose) polymerase-1 cleavage during apoptosis: an update. Apoptosis 2002;7:321–328. [PubMed: 12101391]
26. a Kluck RM, Bossy-Wetzel E, Green DR. The release of cytochrome *c* from mitochondria: a primary site for Bcl-2 regulation of apoptosis. Science 1997;275:1132–1136. [PubMed: 9027315] b Knudson CM, Korsmeyer SJ. Bcl-2 and Bax function independently to regulate cell death. Nat. Genet 1997;16:358–363. [PubMed: 9241272]
27. Satchi-Fainaro R, Puder M, Davies J, Tran H, Greene AK, Corfas G, Folkman J. Targeting angiogenesis with a conjugate of HPMA copolymer and TNP-470. Nat. Med 2004;10:255–261. [PubMed: 14981512]
28. Galbraith SM, Chaplin DJ, Lee F, Stratford MR, Locke RJ, Vojnovic B, Tozer G. M Effects of combretastatin A4 phosphate on endothelial cell morphology in vitro and relationship to tumour vascular targeting activity in vivo. Anticancer Res 2001;21:93–102. [PubMed: 11299795]
29. Ravelli RBG, Gigant B, Curmi PA, Jourdain I, Lachkar S, Sobel A, Knossow M. Insight into tubulin regulation from a complex with colchicine and a stathmin-like domain. Nature 2004;428:198–202. [PubMed: 15014504]
30. Viola G, Fortunato E, Cecconet L, Del Giudice L, Dall'Acqua F, Basso G. Central role of p53 and mitochondrial damage in PUVA-induced apoptosis in human keratinocytes. Toxicol. Appl. Pharmacol 2008;227:84–96. [PubMed: 18048073]
31. Molecular Operating Environment (MOE 2008.10). Montreal, Quebec, Canada: Chemical Computing Group, Inc.; http://www.chemcomp.com.
32. Korb, O.; Stützle, T.; Exner, TE. PLANTS: Application of Ant Colony Optimization to Structure-Based Drug Design. In: Dorigo, M.; Gambardella, LM.; Birattari, M.; Martinoli, A.; Poli, R.; Stützle, T., editors. Ant Colony Optimization and Swarm Intelligence, 5th International Workshop, ANTS 2006; Sep 4–7, 2006; Brussels, Belgium. Berlin: Springer; 2006. p. 247-258.LNCS 4150

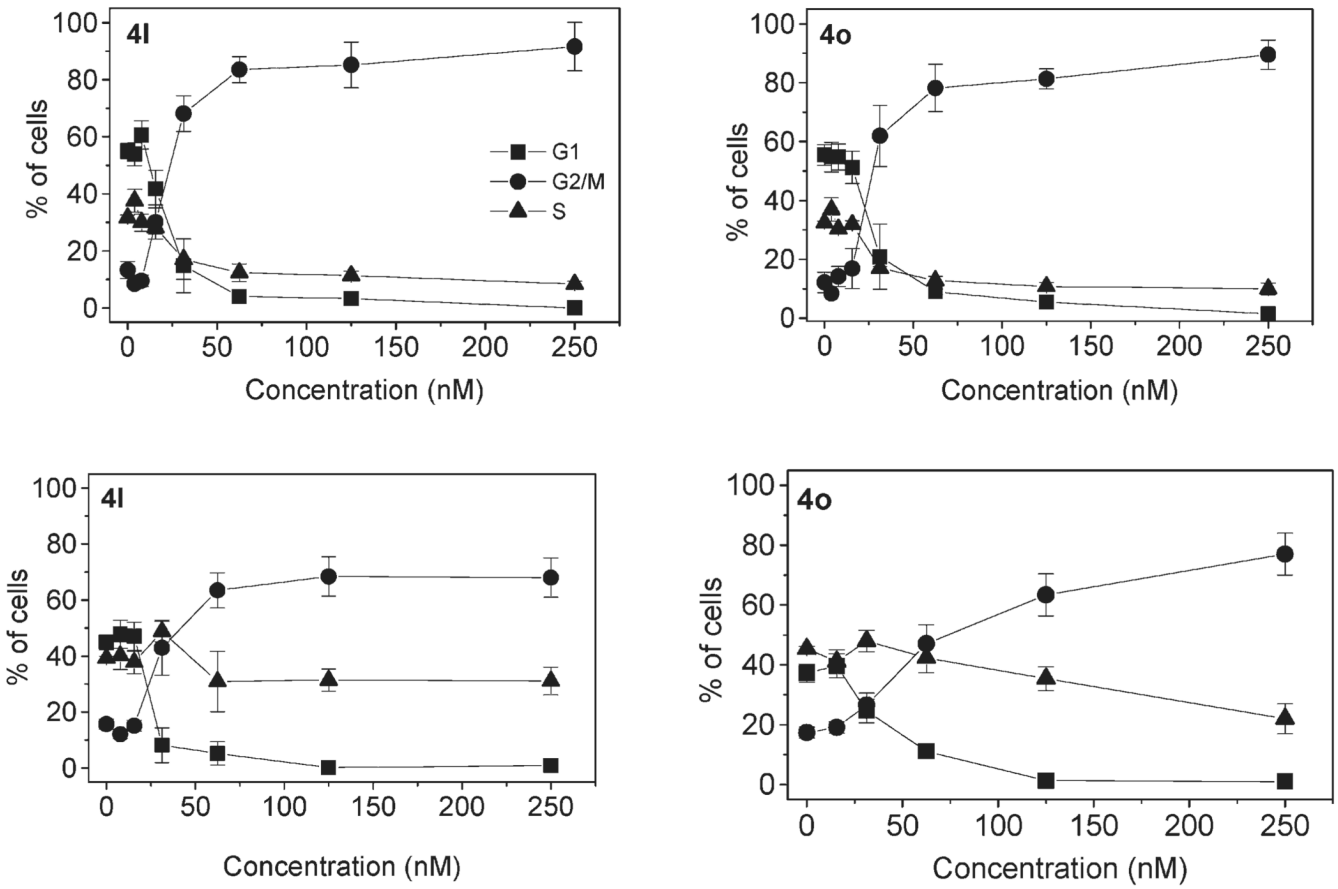

Figure 1.

Effect of **4l** and **4o** induced G2/M phase arrest in HeLa (upper panels) and Jurkat cells (lower panels). Cells were treated with different concentrations ranging from 7 to 250 nM for 24 h. Then the cells were fixed and stained with PI to analyze DNA content by flow cytometry. Data are presented as the mean ± SEM of three independent experiments.

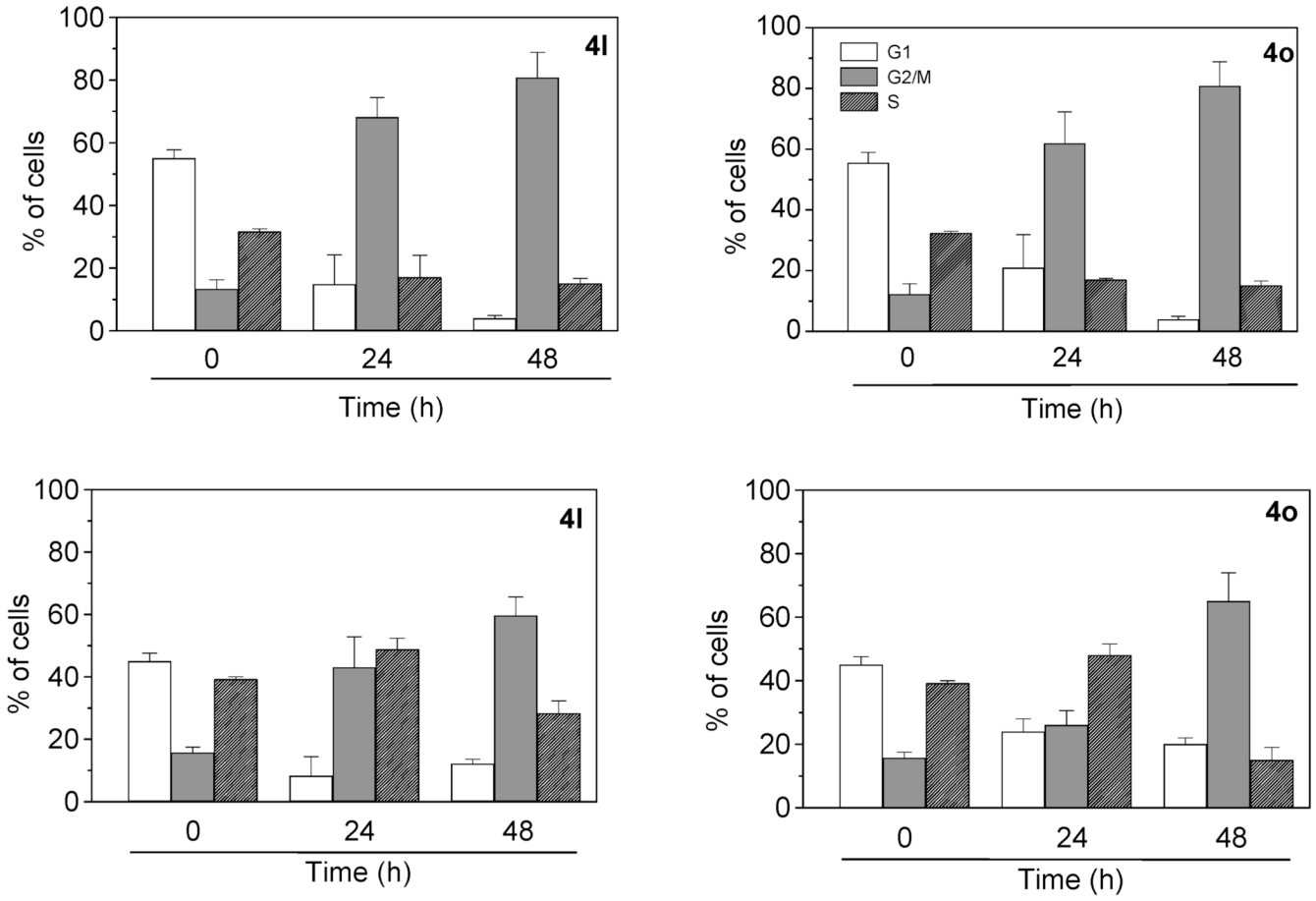

Figure 2.

Effect of **4l** and **4o** induced G2/M phase arrest in HeLa (upper panels) and Jurkat cells (lower panels). Cells were treated with a concentration of 30 nM for 24 and 48 h. Then the cells were fixed and stained with PI to analyze DNA content by flow cytometry. Data are presented as the mean ± SEM of three independent experiments.

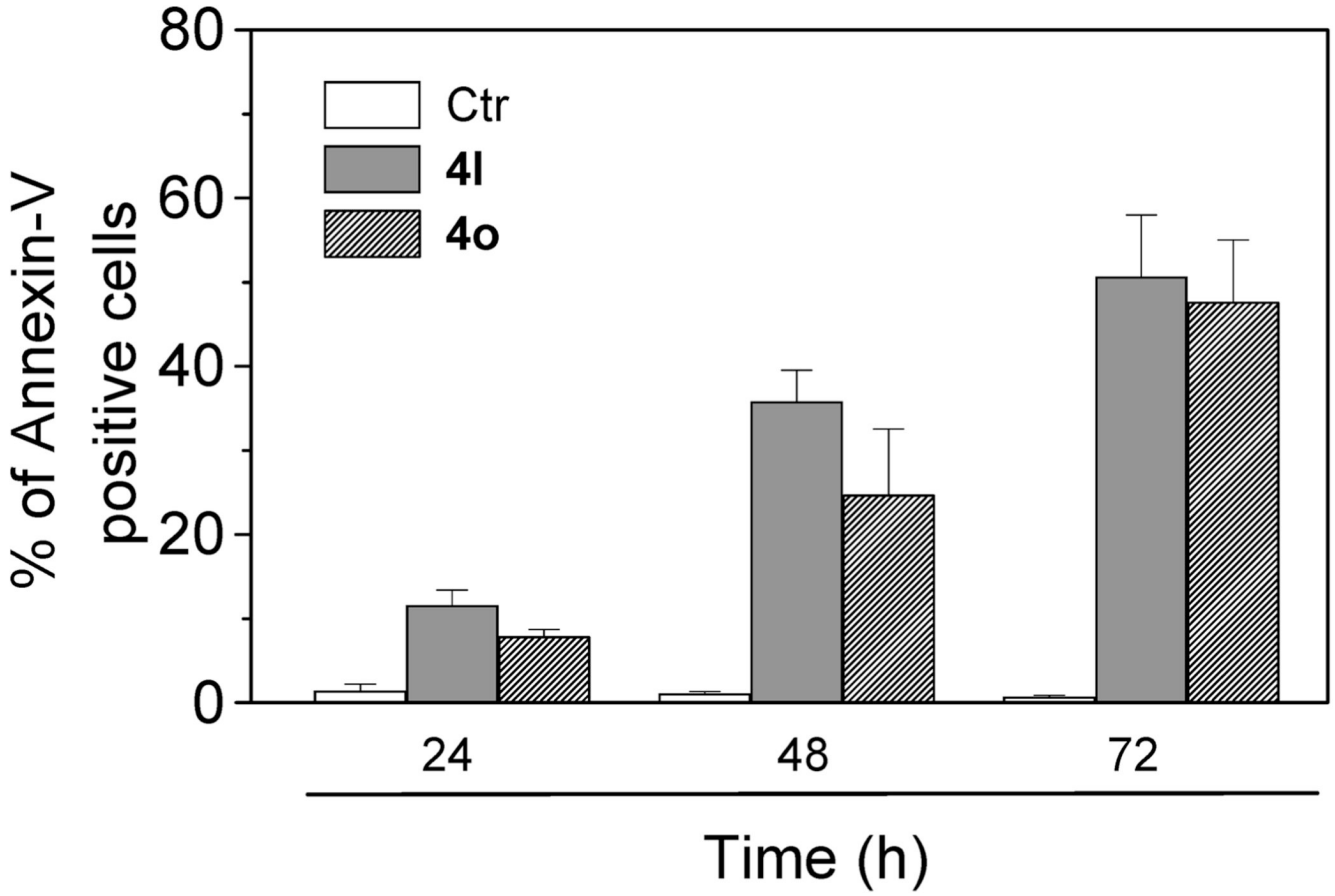

Figure 3.

Flow cytometric analysis of apoptotic cells after treatment of Jurkat cells with **4l** and **4o**. After different times of treatment, cells were harvested and labeled with annexin-V-FITC and PI and then analyzed by flow cytometry. The data are expressed as the mean of percentage of annexin-V positive cells ± SEM for four independent experiments.

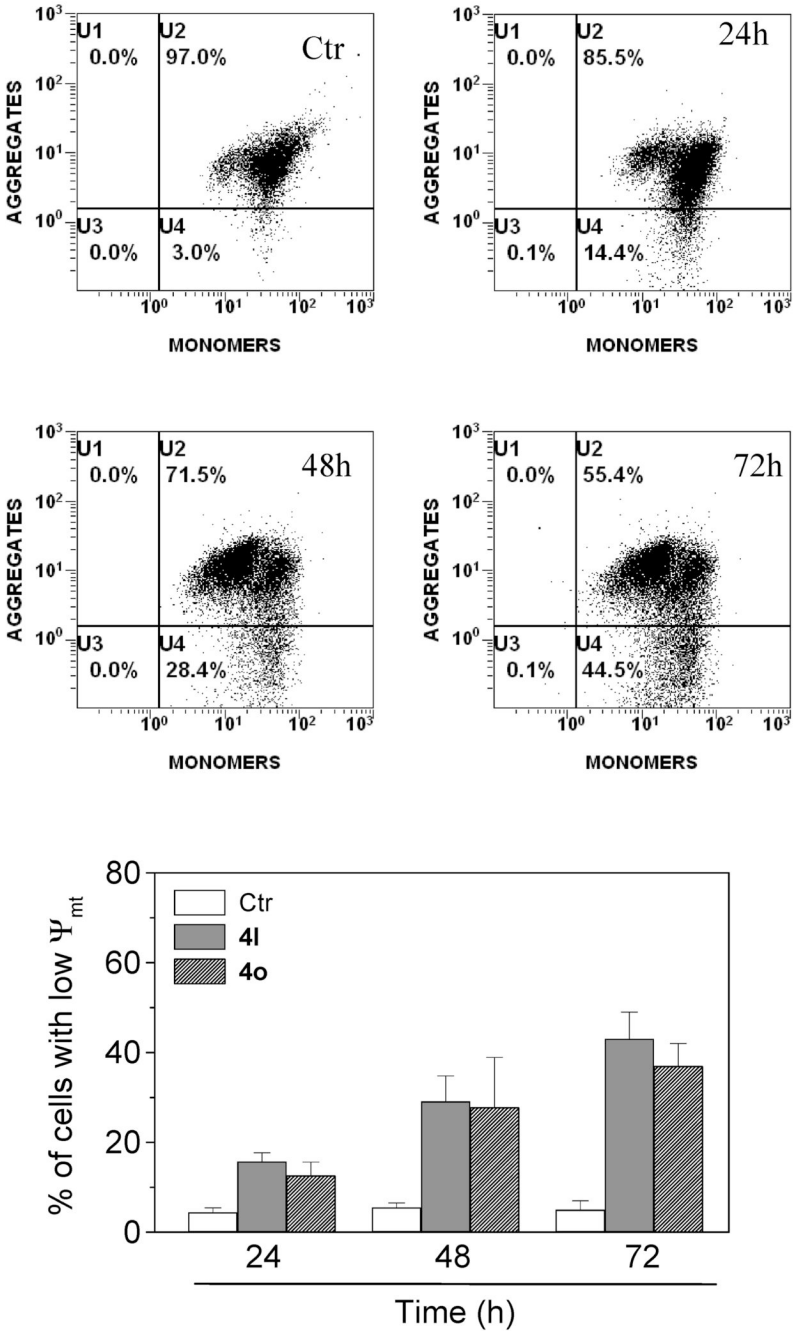

Figure 4.

Assessment of mitochondrial dysfunction after treatment with compound **4l** or **4o**. Upper and middle panels show representative histograms of Jurkat cells treated with 50 nM **4l** for the indicated times and stained with PI and annexin-V-FITC. Lower panel shows induction of loss of mitochondrial membrane potential after 24, 48, and 72 h of incubation of Jurkat cells with 50 nM **4l** or **4o**. Cells were stained with the fluorescent probe JC-1 and analyzed by flow cytometry. Data are expressed as the mean ± SEM for three independent experiments.

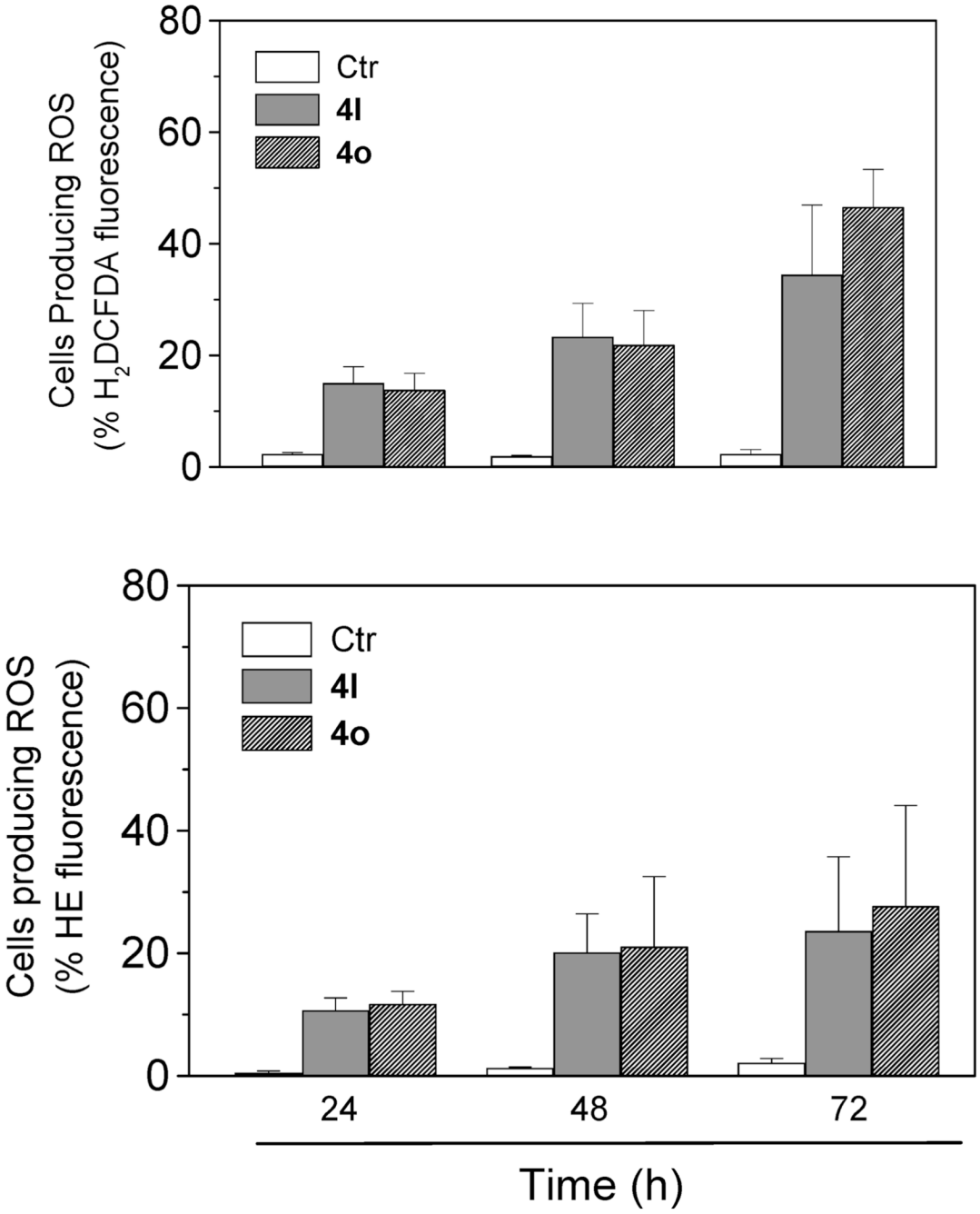

Figure 5.

Mitochondrial production of ROS in Jurkat cells. After 24, 48, and 72 h of incubation with **4l** or **4o**, cells were stained with H_2DCFDA (upper panel) or HE (lower panel) and analyzed by flow cytometry. Data are expressed as the mean ± SEM of three independent experiments.

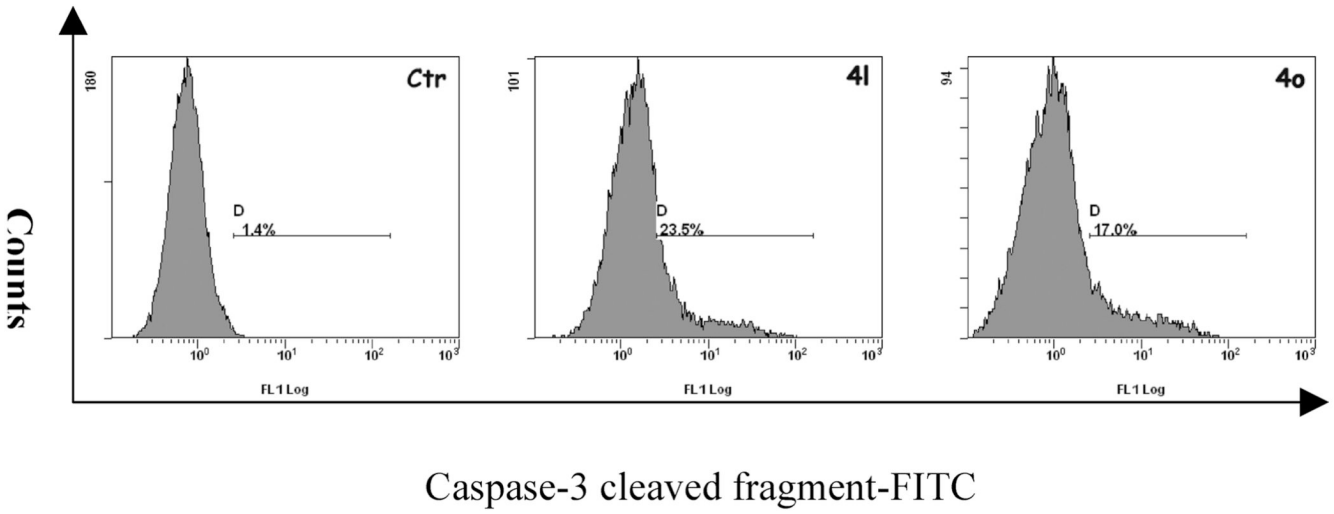

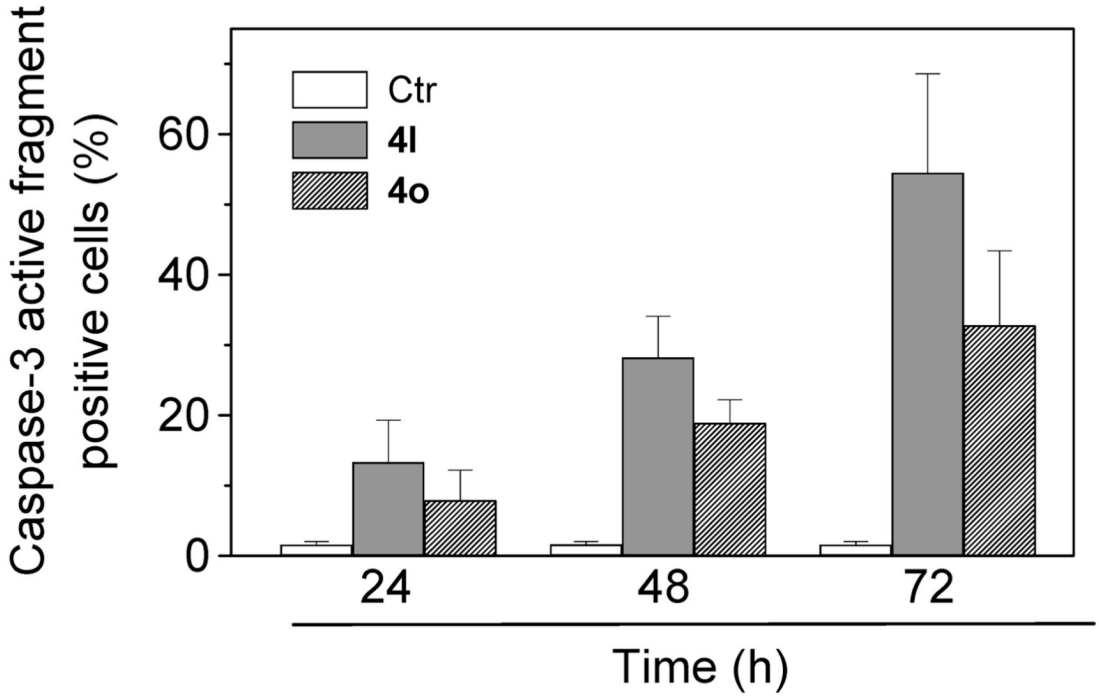

Figure 6.

Caspase-3 induced activity by compound **4l** and **4o**. Jurkat cells were incubated in the presence of **4l** and **4o** at 50 nM. After 24, 48, and 72 h of treatment, cells were harvested and stained with an antihuman active caspase-3 fragment monoclonal antibody conjugated with FITC: (upper panels) representative histograms of Jurkat cells incubated in the presence of 50 nM **4l** and **4o** for 48 h; (lower panel) percentage of caspase-3 active fragment positive cells after 24,48, and 72 h of treatment. Data are expressed as the mean ± SEM of three independent experiments.

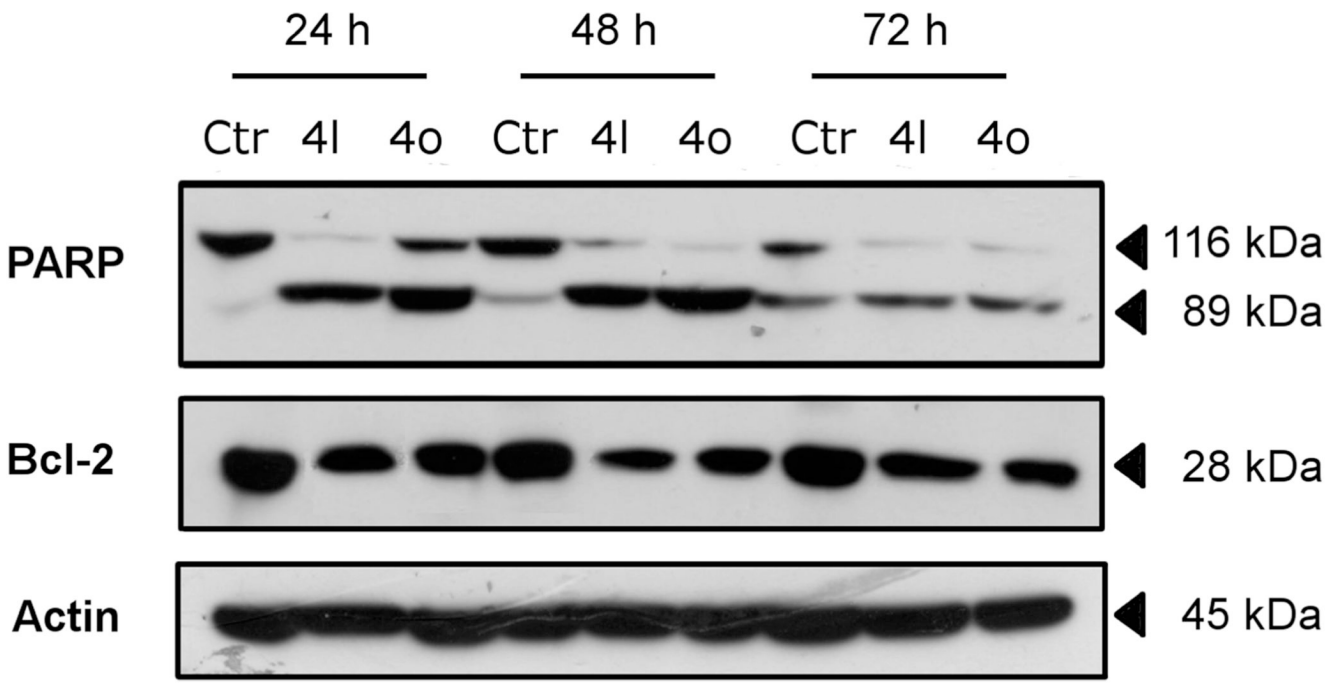

Figure 7.
Western blot analysis for the cleavage of PARP and the expression of Bcl-2 in Jurkat cells. Control lanes (Ctr) refer to untreated cells. In the other lanes the cells were treated with 50 nM **4l** or **4o** for the indicated times. Whole cell lysates were subjected to SDS–PAGE, followed by blotting with an anti-PARP, anti-Bcl-2, or anti-actin antibody.

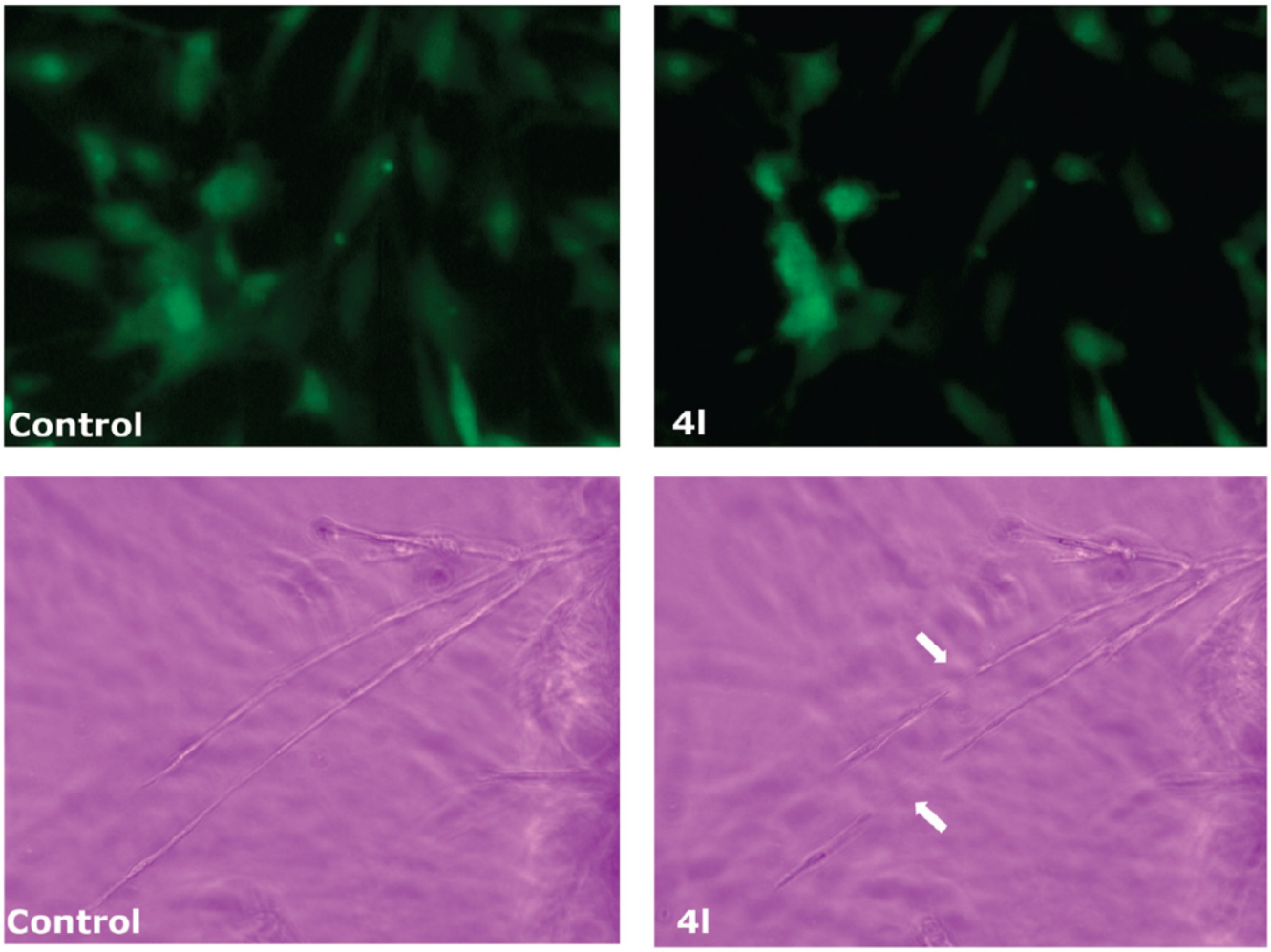

Figure 8.

Effect of compound **4l** on endothelial cell shape in cultured HUVECs (top panels) and chick aortic vascular sprouts (lower panels). Cells or aortic arches from 14-day chick embryos were treated with **4l** and analyzed by confocal microscopy. The left-hand panels are cells prior to compound addition, and the right-hand panels show cells before and after 30 min of treatment with 10 μM **4l.** In the lower panels the arrows indicate the disruption of the aortic vascular sprout induced by drug treatment.

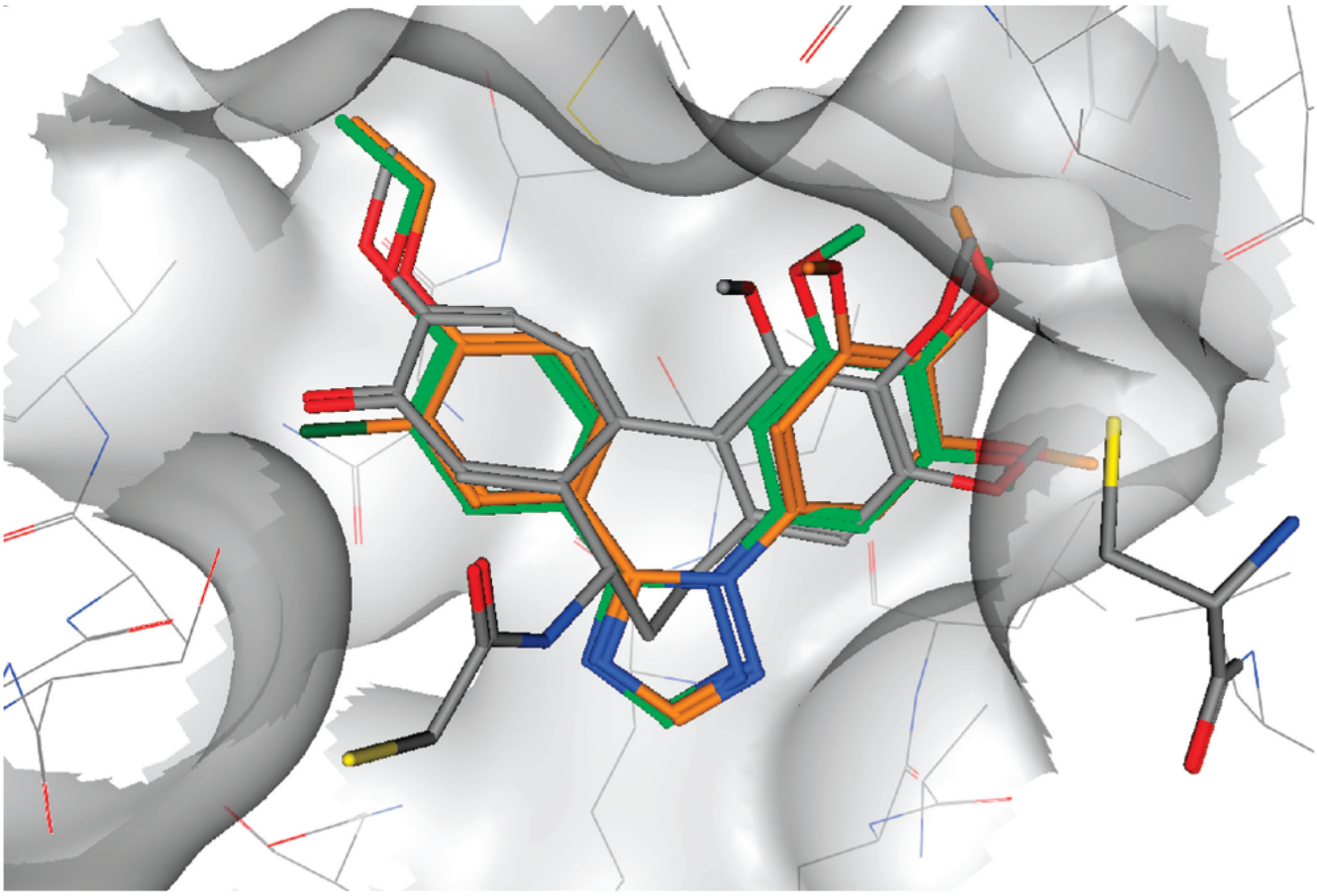

Figure 9.
Presumptive binding mode of compound **4l** (green) and compound **4o** (orange). DAMA-colchicine is shown in gray, and Cys 241 is shown on the right. All compounds and Cys 241 are in stick representation.

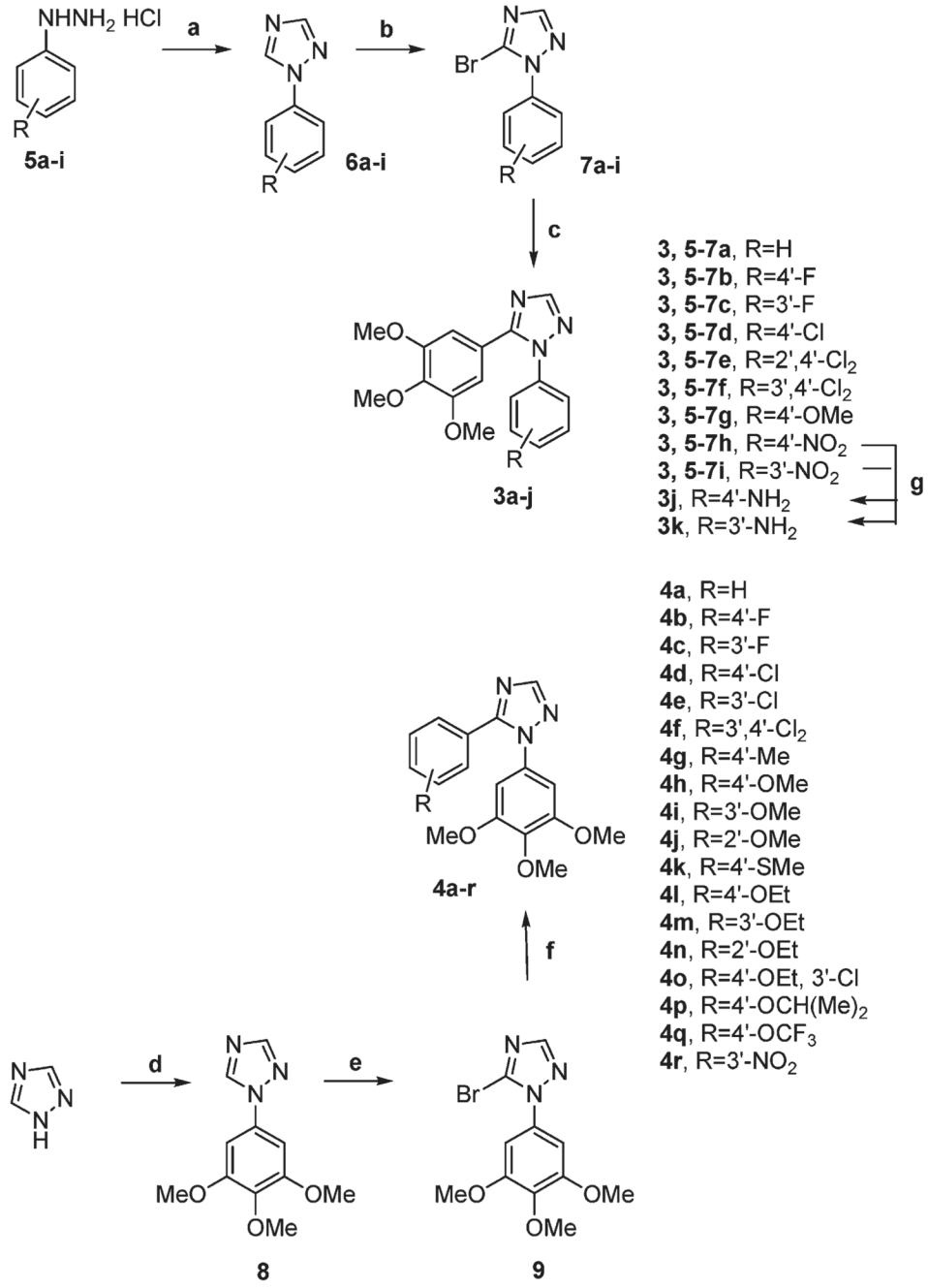

Scheme 1.

[a] Reagents and conditions: (a) $HCONH_2$, 120 °C, 18 h; (b, e) NBS, benzoylperoxide (cat.), CCl_4, reflux; (c, f) $Pd(PPh_3)_4$,K_2CO_3, PhMe, reflux, 18 h; (d) 1-bromo-3,4,5-trimethoxybenzene, $CsCO_3$, CuI, DMF, 120 °C, 18 h; (g) H_2, 10% Pd/C, DMF.

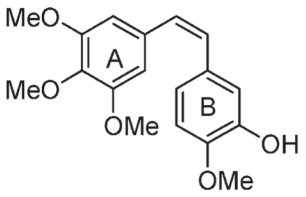

Combretastatin A-4 (CA-4), **1**

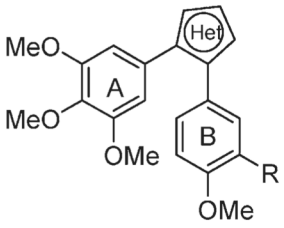

2

R=OH or NH_2
Het=imidazole; pyrazole; thiazole;oxazole; isoxazole; 1,2,3-thiadiazole; 1,2,3- or 1,2,4- or 1,3,4-triazole; 1,2,3,4-tetrazole.

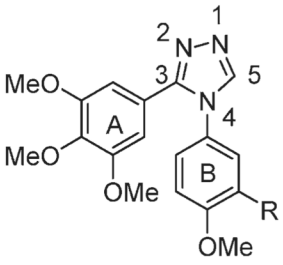

2a, R=H
2b, R=OH
2c, R=F

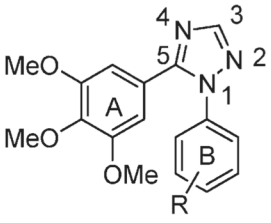

3

3a, R=H
3b, R=4'-F
3c, R=3'-F
3d, R=4'-Cl
3e, R=2',4'-Cl_2
3f, R=3',4'-Cl_2
3g, R=4'-OMe
3h, R=4'-NO_2
3i, R=3'-NO_2
3j, R=4'-NH_2
3k, R=3'-NH_2

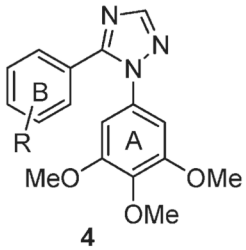

4

4a, R=H
4b, R=4'-F
4c, R=3'-F
4d, R=4'-Cl
4e, R=3'-Cl
4f, R=3',4'-Cl_2
4g, R=4'-Me
4h, R=4'-OMe
4i, R=3'-OMe
4j, R=2'-OMe
4k, R=4'-SMe
4l, R=4'-OEt
4m, R=3'-OEt
4n, R=2'-OEt
4o, R=4'-OEt, 3'-Cl
4p, R=4'-OCH(Me)$_2$
4q, R=4'-OCF_3
4r, R=3'-NO_2

Chart 1.
Inhibitors and Potential Inhibitors of Tubulin Polymerization

Table 1

In Vitro Cell Growth Inhibitory Effects of Compounds **3g**, **4g,h,k,l,o,p**, and CA-4 (**1**)

	IC_{50}[a] (nM)					
compd	**HeLa**	**A549**	**HL-60**	**Jurkat**	**K562**	**MCF-7**
3g	>10000	>10000	6200 ± 1200	93 ± 30	3600 ± 900	7400 ± 1200
4g	250 ± 50	1100 ± 100	90 ± 6	300 ± 80	> 10000	540 ± 20
4h	280 ± 60	520 ± 90	120 ± 10	50 ± 10	950 ± 40	360 ± 50
4k	150 ± 20	800 ± 50	500 ± 20	50 ± 10	340 ± 50	390 ± 90
4l	15 ± 4	100 ± 20	20 ± 3	5 ± 0.2	20 ± 8	50 ± 9
4o	6 ± 2	10 ± 5	3 ± 0.2	3 ± 0.6	20 ± 10	17 ± 1
4p	600 ± 20	>10000	700 ± 200	650 ± 60	800 ± 100	610 ± 10
CA-4	4 ± 1	180 ± 50	1 ± 0.2	5 ± 0.6	5 ± 0.1	370 ± 100

[a] IC_{50}: compound concentration required to inhibit tumor cell proliferation by 50%. Data are expressed as the mean ± SE from the dose–response curves of at least three independent experiments.

Table 2

Inhibition of Tubulin Polymerization and Colchicine Binding by Compounds **3g**, **4g,h,k,l,o,p**, and CA-4

compd	tubulin assembly,[a] IC_{50} ± SD (μM)	colchicine binding,[b] % ± SD
3g	16 ± 1	nd
4g	3.9 ± 0.4	33 ± 6
4h	2.3 ± 0.0	55 ± 1
4k	3.6 ± 0.1	38 ± 3
4l	0.76 ± 0.1	86 ± 2
4o	1.5 ± 0.2	75 ± 0.1
4p	5.1 ± 0.8	37 ± 3
CA-4 (**1**)	1.2 ± 0.1	87 ± 3

[a] Inhibition of tubulin polymerization. Tubulin was at 10 μM.

[b] Inhibition of [^{3}H]colchicine binding. Tubulin, colchicine, and tested compound were at 1, 5, and 1 μM, respectively. nd: not determined.